Forward Models for EEG/MEG

Francoise Lecaignard, J. Mattout

Title MS 330: Forward models for EEG/MEG

Authors Françoise Lecaignard[1,2,3] and Jérémie Mattout[1,2]

Affiliations

[1] Lyon Neuroscience Research Center, Brain Dynamics and Cognition Team, CRNL, INSERM U1028, CNRS UMR5292, Lyon, F-69000, France

[2] University Lyon 1, Lyon, F-69000, France

[3] Cermep - Imagerie du vivant, Lyon, F-69000, France

francoise.lecaignard@inserm.fr
jeremie.mattout@inserm.fr

Synopsys

Like in most inverse problems, where causes have to be inferred from consequences, estimating brain activity from scalp electrophysiological data requires a model. Many EEG/MEG biophysical models have been developed over the last few decades, mostly since the inception of whole head MEG and high density EEG systems. These so-called forward models map neuronal activity onto sensor signals. In this chapter, we briefly cover the main variants and components of these models. They mostly differ by the way they represent neuronal populations, and the way they account for individual anatomy and physical properties. They range from simple (analytical) models to more realistic (numerical) ones. While there is still room for improvement, the question of whether more complex forward models are useful can now be addressed empirically using Bayesian model comparison.

This chapter is made of three sections. The first section describes our current knowledge of what most contributes to EEG/MEG signals and how laws of physics enable us to quantify this contribution. The second section covers the main steps and assumptions that yield the computation of EEG/MEG forward models. It also stresses the main factors of uncertainty in this computation. Finally, the third section emphasizes the difference between the complexity of forward model computation and (probabilistic) model complexity. This notion becomes particularly important when one wants to evaluate different forward models of EEG/MEG data.

I. The origin of EEG and MEG signals

a. From microscopic (single neuron) activity to macroscopic (population level) currents

Neurons have the property to be electrically excitable, to produce and to propagate nerve impulses. Neuronal activity expresses as transmembrane electric currents, which contribute to the macroscopic electric potential differences and magnetic fields measurable on scalp and its vicinity.
Pyramidal and stellate cells are the two main types of neurons. They mostly differ in shape and orientation relative to the cortical surface. Whatever their functional specialization, their typical structure consists of a cell body (soma) surrounded by dendritic branches and extending in a nerve fiber, the axon, which projects onto other neurons through synaptic junctions (Fig.1).
The neuron's membrane contains pores that are selectively permeable to ions.

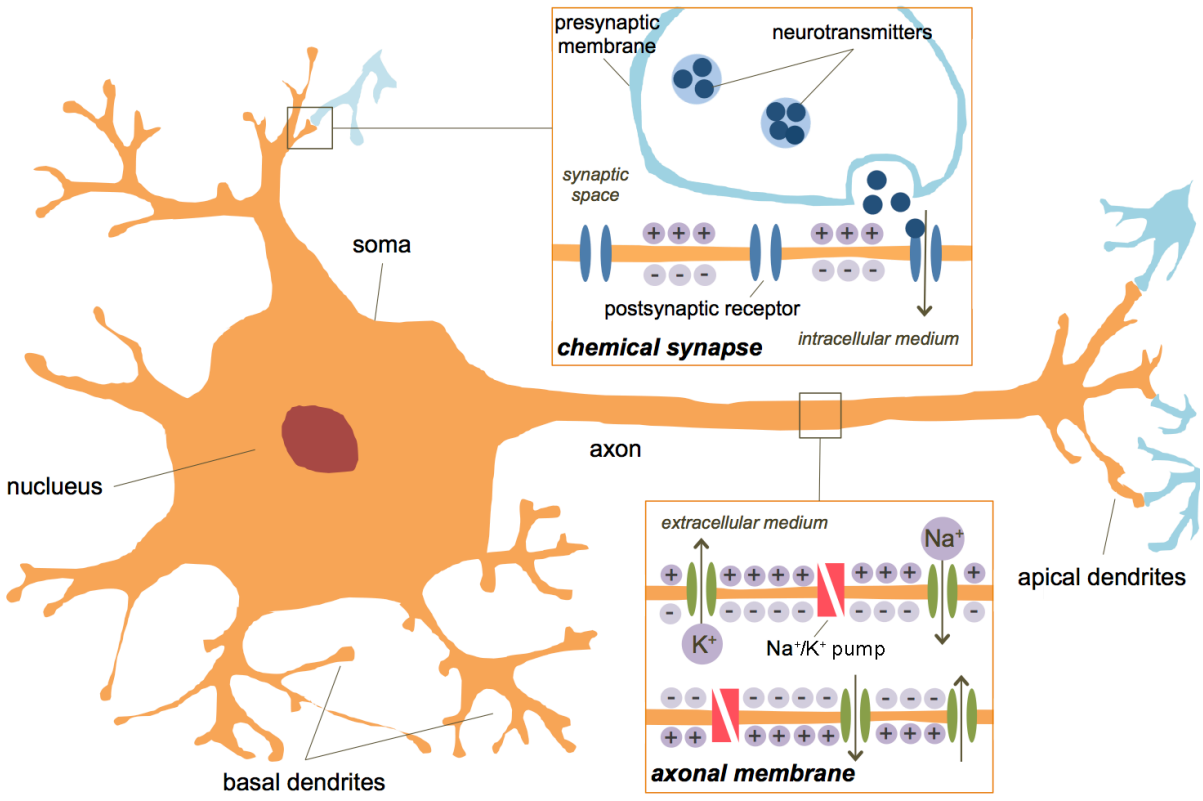

Fig.1. Schematic view of the neuron's structure.

In the absence of excitation, continuous ionic exchanges across the pores maintain the membrane potential V_m at a resting value: $V_m = V_r = V_{intra} - V_{extra} \approx -70mV$.

Typical dendrites receive inputs from pre-synaptic neurons by way of a chemical exchange called ***neurotransmission***. Fixation of released neurotransmitters on post-synaptic receptors triggers the opening of specific pores, allowing for ionic movements across the membrane. These currents cause the ***post-synaptic*** (membrane) ***potentials*** (PSP). Synaptic integration of PSP over time and space results in an ***action potential*** (AP) propagating along the axon towards the apical dendrites, upon condition that a depolarization threshold has been reached ($V_m > V_t \approx -50mV$). Excitatory synapses tend to evoke a local membrane depolarization ($V_m > V_t$), whereas inhibitory synapses cause local membrane hyperpolarization ($V_m < V_t$).

From the extracellular medium, a site along the membrane where ions move into the cell corresponds to a ***sink current*** (current disappearance), whereas a site where ions go out of the cell defines a ***source current*** (current appearance). Transmembrane and intracellular currents are grouped together at the micro- (neuronal) scale and more generally at the meso- (cell assembly) scale to form the ***primary currents*** J_p, often described as currents related to postsynaptic activity. They produce an electric field in the medium, which in turn gives rise to ***conduction currents*** $J_e = \sigma E$, also referred to as volume or secondary currents. In every point within the head, the electric current can be described as $J = J_p + \sigma E$.

Source and sink current distributions on the membrane can be modeled by multipolar (Taylor) developments (Mosher, Leahy, Shattuck and Baillet, 1999). Simple dipole models capture well the contribution of PSPs (Koles, 1998), whereas APs are well described by quadrupole models whose contribution decreases rapidly with distance and can be neglected in the context of EEG and MEG (Crouzeix, 2001) (Fig. 2). Furthermore, approximately 50,000 neurons with simultaneous activity and similar orientation are required to be picked up by MEG and EEG sensors (Pernier, 2007). Consequently, it is usually assumed that only the primary currents produced by a synchronous population of neurons with a preferred orientation such as the pyramidal cells contribute to the electric potentials and magnetic fields measurable on scalp (Crouzeix, 2001; Nunez, 1981).

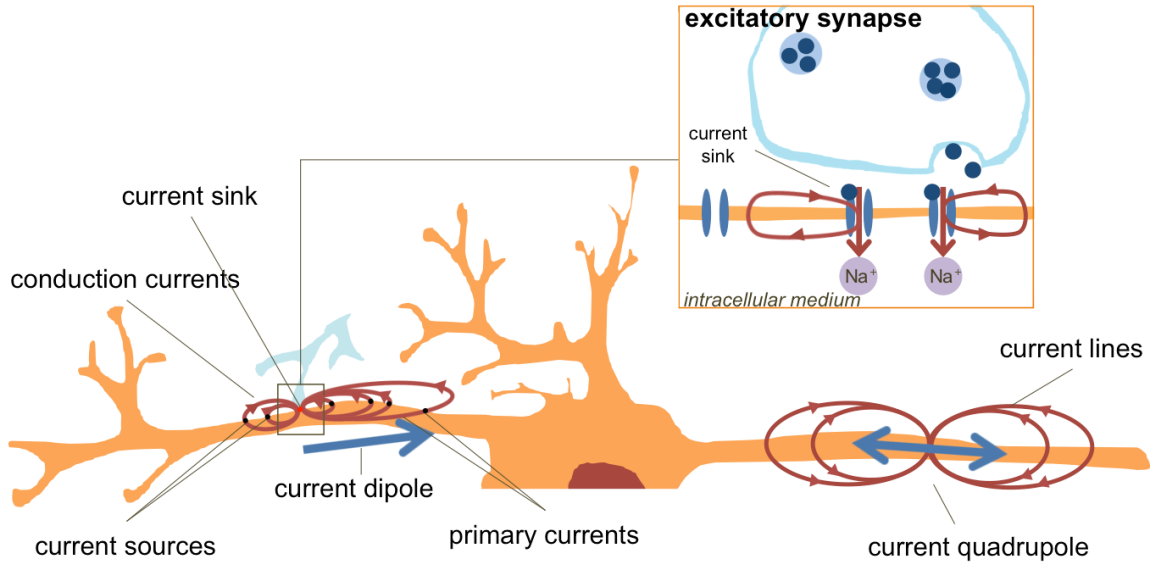

Fig.2. Schematic view of neuronal current distributions. An excitatory synapse creates a local sink current, which induces primary currents across the membrane and within the cell. The conducting currents close the loop in the extracellular space, hence creating a distribution of source currents along the membrane. In the same way, an inhibitory synapse creates a source current.

b. From macroscopic currents to observed electric and magnetic fields

Predicting the electric ($\vec{E}$) and magnetic ($\vec{B}$) fields produced by neuronal activity on EEG and MEG sensors requires solving Maxwell's equations in head tissues. In their general form, Maxwell's equations write:

$$\nabla.\vec{E} = \frac{\rho}{\varepsilon} \qquad \nabla \wedge \vec{E} = -\frac{\partial \vec{B}}{\partial t} \qquad \nabla.\vec{B} = 0 \qquad \nabla \wedge \vec{B} = \mu\left(\vec{J} + \varepsilon \frac{\partial \vec{E}}{\partial t}\right) \tag{1.1}$$

where $\vec{J}$ and ρ indicate the volume density of current and volume density of charge, respectively. ε and μ are the electric permittivity and magnetic permeability of the medium, respectively.

The head is composed of several tissues with various conductivities and therefore can be described as a finite inhomogeneous conducting volume. It is commonly accepted that ε and μ are equal to free space value (ε_0 and μ_0 respectively) (Malmivuo and Plonsey, 1995). Given the frequency spectra of EEG and MEG signals is much below 1 kHz, capacitive effects can be neglected (Schwan and Kay, 1957). The duration of the electromagnetic wave propagation (from neuronal sources to sensors) is negligible compared to physiological time constants, hence scalp measures appear as instantaneous and synchronous, and the quasi-static approximation holds (Plonsey and Heppner, 1967). Under this regime, Maxwell's equations simplify as follows:

$$\nabla.\vec{E} = \frac{\rho}{\varepsilon_0} \qquad \nabla \wedge \vec{E} = \vec{0} \qquad \nabla.\vec{B} = 0 \qquad \nabla \wedge \vec{B} = \mu_0 \vec{J} \tag{1.2}$$

The electric and magnetic fields are now decoupled and importantly, the forward computation has become independent of time. The later means that only the location, orientation and amplitude of the neuronal sources need to be known to compute the sensor signals.

Since the electric potential simply relates to the electric field by

$$\vec{E}(r,t) = -\overrightarrow{grad}(V(r,t)) \tag{1.3}$$

and accounting for Ohm's law, the law of conservation of charge and Biot-Savart's law which relates magnetic fields to the underlying currents, equations (1.2) yield the following formulations for the electric potential **V(r,t)** and the magnetic field **B(r,t)** distributions, given a time-varying source distribution **Jp(r,t)** and tissue conductivity **σ(r)**:

$$\sigma(r)\nabla.\overrightarrow{grad}(V(r,t) = \nabla.\overrightarrow{J_p}(r,t) \tag{1.4}$$

$$B(r,t) = \frac{\mu_0}{4\pi}\int \frac{\left[\overrightarrow{Jp}(r',t) - \sigma(r')\overrightarrow{grad}(V(r',t))\right] \wedge (\vec{r}' - \vec{r})}{\left|r' - r\right|^3} dr' \tag{1.5}$$

at spatial location *r* and time *t*. Difference between EEG and MEG data generated by the same underlying sources are illustrated in Fig.3.

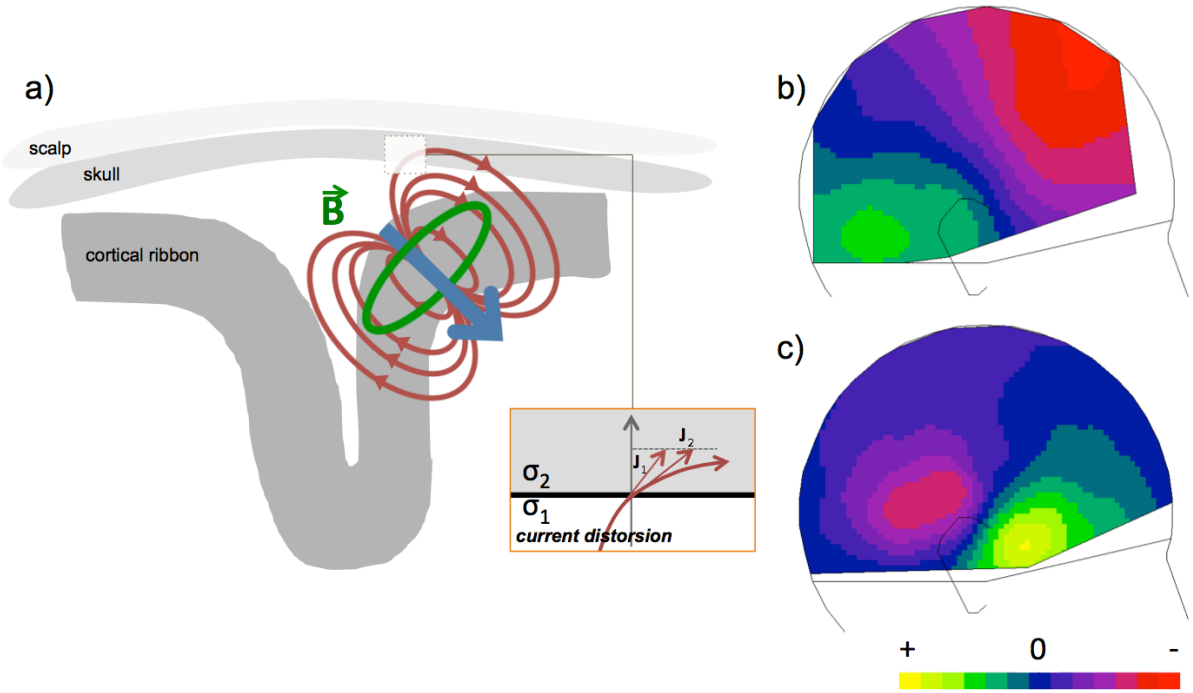

Fig.3. a). Current dipole with electric field lines (red) and magnetic field lines (green). Because of different conductivities in different head tissues, current lines are distorted when they cross tissue boundaries (figure adapted from [2]).b) Scalp topography of real EEG data (auditory evoked response N100). c) Corresponding scalp topography of MEG data (from simultaneously recorded EEG and MEG responses to auditory tones).

II. The main forward model assumptions

A forward model of EEG and MEG data calls for a description of the neuronal current distribution (referred to as the source distribution), a specification of the conducting properties of the head tissues and some information about the sensors (locations and orientations in the case of MEG). A large number of models have been proposed in the literature. They differ by the realism with which they account for the physical and geometrical properties of head tissues. In other words, the practicality of deriving EEG and MEG forward models often boils down to trading off between the complexity of computing a fine individual structural and physical model, and the accuracy of the ensuing forward prediction. In addition, contrary to simple models, complex ones will not have analytical solutions and numerical approximations will be needed.

a. The source model

At the macro-scale, the coherent activity of a neuronal assembly is most commonly modeled by an ***equivalent current dipole (ECD)*** (Fig. 3a). Higher order models have also been explored (Nolte and Curio, 2000), mostly as an attempt to better capture the extent of active cortical areas. However, such models introduce a higher number of unknown parameters that are also difficult to interpret. Nevertheless, quadrupoles may be of interest, particularly in MEG, to model the complex fields generated by extended and deep cortical sources (Jerbi et al., 2004).

Two main approaches can be distinguished when considering the ECD as a unitary source model:

- **The dipolar approach** relies on the assumption that a fairly small number of ECDs (fixed a priori, typically less than 8) contribute simultaneously and significantly to the scalp data. Each ECD is fully described by 6 parameters, 3 for its location and 3 for its orientation and magnitude. This yields a well-conditioned system where the number of unknown parameters to be fitted is smaller than the number of independent data points (which at each point in time roughly corresponds to the number of sensors).

- **The distributed or imaging approach** relaxes the strong constraint on the number of active regions. A few thousands ECDs are typically used to model the entire source space with fixed positions, either distributed over a 3D regular grid covering the whole brain volume or limited to the cortical sheet with a possible normal orientation constraint. For the latter, only each ECD magnitude is left to be estimated, yielding a linear but ill-conditioned system to be solved. A unique solution to the ill-posed EEG/MEG inverse problem will be obtained here by incorporating additional constraints about the source configuration (see Chapter 331). This source model enables one to produce images of cortical or brain activity, which makes statistical inference at the subject or group level more tractable and more sensitive (Mattout, Henson and Friston, 2007; Litvak and Friston, 2008).

b. The head model

This is another critical part of the forward model. It embeds our knowledge and assumptions on head tissue geometry and conducting properties.

- **Head geometry models**

Spherical models are the simplest ones, consisting of concentric spheres with homogeneous and isotropic conductivity in each compartment or layer (Rush and Driscoll, 1968; de Munck, van Dijk and Spekreijse, 1988). Although the head is not spherical, these models are attractive because of the ensuing exact analytic expressions for the electric potential and magnetic field on the head surface. They have been extensively evaluated empirically.

The **"3 shell"** model distinguishes between the scalp, skull and brain layers with radius ratio and isotropic conductivities as proposed in (Rush and Driscoll, 1969). It is largely used for EEG and available in most routine softwares.
Since the magnetic permeability is homogenous over tissues and volume currents barely contribute to the external magnetic field, spherical models appear more suitable for MEG than EEG. MEG spherical models are blind to volume currents contributions but present the advantage that neither tissue conductivity knowledge nor the radius of the sphere is needed. The **"overlapping spheres"** model, which refines the single sphere model by fitting a sphere to each sensor location, provides a better MEG forward solution (Huang, Mosher and Leahy, 1999).

Realistic models are numerical models that have been mostly developed for EEG, to better account for the shape and electrical properties of the tissues, namely their electrical conductivity as with the **Boundery Element Method (BEM)** (Hämäläinen and Sarvas, 1989) and their anisotropy as with the **Finite Element Method (FEM)** (Marino et al., 1993) or the **Finite Difference Method (FDM)** (Lemieux, McBride and Hand, 1996).
The BEM relies on surface meshes derived from MRI segmentation and assigns each layer with homogenous and isotropic conductivity. Studies comparing spherical and BEM models in EEG and MEG obtained better source estimates using BEM for dipoles below the supratemporal plane (Yvert et al., 1997; Crouzeix, Yvert, Bertrand and Pernier, 1999).FEM and FDM rely on 3D meshes where each finite element can be ascribed with a different, anisotropic conductivity tensor matrix. Models then differ in their number of compartments, conductivity values, anisotropic ratios and tensor orientations. The latter can be derived from Diffusion Tensor Imaging (DTI) (Tuch et al., 2001).

We refer the reader to (Rush and Driscoll, 1969; Sarvas, 1987; Meijs, Weier, Peters and van Oosterom, 1989; Hämäläinen et al., 1993; Mosher, Leahy and Lewis, 1999) for a detailed description of the forward model computation, under the spherical assumption (analytic form) and the more realistic assumption (numerical form).

- **Head tissue conductivities**

Individual conductivity values are of high importance, particularly for realistic models. Estimations from dead tissues have proved very different from *in vivo* values and first in vivo observations have come from anaesthetized animals (Robillard and Poussart, 1977). More recently, *in vivo* measures have been made possible in humans thanks to the advent of Electric Impedance Tomography (EIT) (Ferree, Eriksen and Tucker, 2000; Gonçalves et al., 2000) as well as Diffusion Tensor Imaging (DTI) (Tuch et al., 1999) but these techniques can still hardly be used routinely. Hence empirical values reported in experimental studies are largely used as a first approximation (Rush and Driscoll, 1968). Several studies based on simulated data have compared the relative sensitivity of EEG and MEG forward solutions to conductivities. Critically, EEG is highly sensitive to the brain/skull conductivity ratio (Vallaghé and Clerc, 2009) as well as to white matter anisotropy (Güllmar, Haueisen and Reichenbach, 2010). MEG is particularly sensitive to brain tissue conductivity (Gencer and Acar, 2004; Van Uitert and Johnson, 2003) and white matter anisotropy (Güllmar, Haueisen and Reichenbach, 2010).

c. Sensor registration

Sensor description relative to the head model is achieved by means of a spatial transformation based on head landmarks (least-square fitting) or head surface (surface-matching methods) or both, identified in both the MRI and the electrophysiological coordinate systems.

Various sources of errors are associated with sensor coregistration, particularly landmark identification on MR images, electrode and landmark digitization and head movements during MEG acquisition. Typically, coregistration errors range between 5 and 10 mm (Whalen, Maclin, Fabiani and Gratton, 2008; Hillebrand and Barnes, 2011), with moderate

consequences on EEG inverse solutions (Wang and Gotman, 2001; Acar and Makeig, 2013) but potentially dramatic effects on MEG ones (Hillebrand and Barnes, 2003). Interestingly, uncertainty about the forward model, due to coregistration, could be accounted for in the source reconstruction process thanks to probabilistic or Bayesian methods (López, Penny, Espinosa and Barnes, 2012).

III. Empirical evaluation of forward model assumptions

a. From forward to generative models

The forward relationship between source parameters θ and observed EEG or MEG data Y is of the general form

$$Y = L(\theta) \qquad (3.1)$$

where L indicates the lead-field operator and embodies all the pre-cited anatomical and biophysical assumptions one needs to account for in the forward model. Data Y is a $N * T$ matrix, where N is the number of sensors and T the number of time samples. θ is a P-long vector made of all source location, orientation and amplitude parameters.

Forward models have in themselves barely no interest; they are only useful and even mandatory when one aims at reconstructing brain activity from scalp recordings, that is inverting equation (3.1) to estimate θ. Contrary to the forward computation of L, this inverse problem is ill-posed and requires additional (prior) information or constraints to ensure a unique solution (see chapter 331). Two types of additional assumptions can be specified: assumptions about measurement noise and prior knowledge about parameters θ. In particular, when source locations are fixed as in distributed approaches, equation (3.1) becomes linear:

$$Y = L.\theta + \varepsilon \qquad (3.2)$$

where L is the $N * P$ lead-field (or gain) matrix operator and ε models an additive measurement noise which is usually assumed to follow a Gaussian distribution with zero mean and a fully known or parameterized variance structure (Mattout et al., 2006).

This highlights the fact that solving the inverse problem requires the specification of not only the lead-field operator L but also of the prior distributions over noise ε and parameters θ. Altogether, those assumptions make a full generative model, which could be used to simulate realistic EEG or MEG data.

The probabilistic or Bayesian framework is very much appropriate to define and invert generative models. Indeed, probabilistic distributions can flexibly describe our knowledge or uncertainty about a phenomenon. Moreover, advanced inference techniques have been developed to invert complex probabilistic models (see chapter 325).

b. Bayesian (forward) model comparison

Importantly, the Bayesian framework enables formal model comparison given empirical observations. Since the forward model is part of the generative model, Bayesian model comparison offers a principled way to compare forward model assumptions, as long as all other assumptions (namely priors over noise and source parameters) are kept the same for each compared generative model, and provided that all models are fitted to the same dataset.

This is a recent and important extension to previous evaluation approaches of EEG and MEG forward models which mostly rested on numerical simulations (Crouzeix et al., 1999; Vatta et al., 2010; Acar and Makeig, 2013) and on a few empirical measures using biophysical phantoms (Leahy et al., 1998; Baillet et al., 2001).

Bayesian model comparison rests on computing the model evidence $p(Y|M)$ (see chapter 328). The higher the model evidence, the better the model. A useful approximation to the log-evidence is the Free energy (F) (Penny, 2012). It can be obtained using variational techniques (see Chapter 327) and has already been used to compare forward models of EEG and MEG data.
Namely, it could show that canonical cortical meshes may carry sufficient structural information to solve the MEG inverse problem (Mattout, Henson and Friston, 2007; Henson, Mattout, Phillips and Friston, 2009).

c. A note on model complexity

Given data Y and model M with parameters θ, the free energy writes

$$F = \langle \ln p(Y|\theta, M) \rangle_q - KL\big(q(\theta)\big|p(\theta|M)\big) \qquad (3.3)$$

where

- $p(Y|\theta, M)$ and $p(\theta|M)$ are the likelihood and prior distributions, respectively. They fully define the generative model M.
- $q(\theta)$ is the approximate posterior distribution over model parameters (the outcome of the inverse inference process).
- KL is the Kullback-Leibler divergence which can be interpreted as a statistical distance between two distributions. Here, it quantifies the distance between the posterior and the prior distribution over θ.

Importantly, the first term in equation (3.3) corresponds to model accuracy, while the second term quantifies model complexity. In the general case of Gaussian distributions, this term writes

$$KL\big(q(\theta)\big|p(\theta|M)\big) = \frac{1}{2}\ln|C_\theta| - \frac{1}{2}\ln|C_{\theta/Y}| + \frac{1}{2}\big(\mu_{\theta/Y} - \mu_\theta\big)^T C_\theta{}^{-1}\big(\mu_{\theta/Y} - \mu_\theta\big) + Trace\left(C_\theta{}^{-1} C_{\theta/Y}\right) + cst \qquad (3.4)$$

where μ_θ, C_θ and $\mu_{\theta/Y}$, $C_{\theta/Y}$ are the mean and variance of the prior and posterior distributions, respectively.

Given those equations, changing the lead-field operator by moving from a simple spherical head model to a more realistic one might increase the free energy in two ways:

- by improving the fit of the data (increasing model accuracy);
- by reducing model complexity through a posterior distribution that would decrease the above Kullback-Leibler divergence. Namely, this could be the case if the realistic model would yield a smaller posterior correlation between parameters (Penny, 2012).

Importantly, this means that a more realistic model, although more complex in a computing sense (because it requires the fine extraction of individual anatomical and biophysical features) might yield a significantly higher free energy.

However, this will be the case only if such a model offers a more realistic and higher spatial resolution that the data can accommodate. In other words, whether it is worth deriving a fine and realistic head model for source reconstruction depends on the spatial precision that the data can offer.
In (Henson et al., 2009), using data from a face perception MEG experiment; it was shown that a BEM model should be preferred to a spherical one, provided individually-defined inner skull and scalp meshes were used.

Finally, beside head models, Bayesian model comparison can also be used to evaluate the ability of EEG and MEG data to inform advanced source models based on neural masses. Recent developments of Dynamic Causal Models to study brain effective connectivity have led to more biologically plausible models of neuronal populations. As an example, a recent study suggests that EEG data can distinguish between the dynamics of local neuronal excitatory and inhibitory subpopulations (Moran et al., 2013).

Related chapters

7. EEG

12. MEG

325. Bayesian Model Inversion

327. Variational Bayes

328. Bayesian Model Selection

331. Distributed Bayesian Inversion of MEG/EEG models

333. Neural mass models

340. Dynamic Causal Models for EEG

References

Acar, Z.A. and Makeig, S. 2013. Effects of Forward Model Errors on EEG Source Localization. *Brain Topography*, 26(3), pp.378–396.

Baillet, S., Riera, J.J., Marin, G., Mangin, J.F., Aubert, J. and Garnero, L. 2001. Evaluation of inverse methods and head models for EEG source localization using a human skull phantom. *Physics in Medicine and Biology*, 46(1), pp.77–96.

Crouzeix, A. 2001. ***Méthodes de localisation des générateurs de l'activité électrique cérébrale à partir de signaux électro- et magnéto-encéphalographiques.*** pp.1–264.

Crouzeix, A., Yvert, B., Bertrand, O. and Pernier, J. 1999. An evaluation of dipole reconstruction accuracy with spherical and realistic head models in MEG. *Clinical neurophysiology : official journal of the International Federation of Clinical Neurophysiology*, 110(12), pp.2176–2188.

de Munck, J.C., van Dijk, B.W. and Spekreijse, H. 1988. Mathematical dipoles are adequate to describe realistic generators of human brain activity. *IEEE transactions on bio-medical engineering*, 35(11), pp.960–966.

Ferree, T.C., Eriksen, K.J. and Tucker, D.M. 2000. Regional head tissue conductivity estimation for improved EEG analysis. *IEEE transactions on bio-medical engineering*, 47(12), pp.1584–1592.

Gencer, N.G. and Acar, C.E. 2004. Sensitivity of EEG and MEG measurements to tissue conductivity. *Physics in Medicine and Biology*, 49(5), pp.701–717.

Gonçalves, S., de Munck, J.C., Heethaar, R.M., Lopes da Silva, F.H. and van Dijk, B.W. 2000. The application of electrical impedance tomography to reduce systematic errors in the EEG inverse problem--a simulation study. *Physiological measurement*, 21(3), pp.379–393.

Güllmar, D., Haueisen, J. and Reichenbach, J.R. 2010. Influence of anisotropic electrical conductivity in white matter tissue on the EEG/MEG forward and inverse

solution. A high-resolution whole head simulation study. *NeuroImage*, 51(1), pp.145–163.

Hämäläinen, M.S. and Sarvas, J. 1989. Realistic conductivity geometry model of the human head for interpretation of neuromagnetic data. *IEEE transactions on bio-medical engineering*, 36(2), pp.165–171.

Hämäläinen, M.S., Hari, R., Ilmoniemi, R.J., Knuutila, J. and Lounasmaa, O. 1993. Magnetoencephalography - theory, instrumentation, and applications to noninvasive studies of the working human brain. *Reviews of Modern Physics*, 65(2), pp.413–497.

Henson, R.N., Mattout, J., Phillips, C. and Friston, K.J. 2009. Selecting forward models for MEG source-reconstruction using model-evidence. *NeuroImage*, 46(1), pp.168–176.

Hillebrand, A. and Barnes, G.R. 2003. The use of anatomical constraints with MEG beamformers. *NeuroImage*, 20(4), pp.2302–2313.

Hillebrand, A. and Barnes, G.R. 2011. Practical constraints on estimation of source extent with MEG beamformers. *NeuroImage*, 54(4), pp.2732–2740.

Huang, M.X., Mosher, J.C. and Leahy, R.M. 1999. A sensor-weighted overlapping-sphere head model and exhaustive head model comparison for MEG. *Physics in Medicine and Biology*, 44(2), pp.423–440.

Jerbi, K., Baillet, S., Mosher, J.C., Nolte, G., Garnero, L. and Leahy, R.M. 2004. Localization of realistic cortical activity in MEG using current multipoles. *NeuroImage*, 22(2), pp.779–793.

Koles, Z.J. 1998. Trends in EEG source localization. *Electroencephalography and clinical neurophysiology*, 106(2), pp.127–137.

Leahy, R.M., Mosher, J.C., Spencer, M.E., Huang, M.X. and Lewine, J.D. 1998. A study of dipole localization accuracy for MEG and EEG using a human skull phantom. *Electroencephalography and clinical neurophysiology*, 107(2), pp.159–173.

Lemieux, L., McBride, A. and Hand, J.W. 1996. Calculation of electrical potentials on the surface of a realistic head model by finite differences. *Physics in Medicine and Biology*, 41(7), pp.1079–1091.

Litvak, V. and Friston, K.J. 2008. Electromagnetic source reconstruction for group studies. *NeuroImage*, 42(4), pp.1490–1498.

López, J.D., Penny, W.D., Espinosa, J.J. and Barnes, G.R. 2012. A general Bayesian treatment for MEG source reconstruction incorporating lead field uncertainty. *NeuroImage*, 60(2), pp.1194–1204.

Malmivuo, J. and Plonsey, R. 1995. *Bioelectromagnetism*. New-York: Oxford University Press.

Marino, F., Halgren, E., Badier, J.-M., Gee, M. and Nenov, V. 1993. A finite difference model of electric field propagation in the human head : implementation and validation. th IEEE annual Northeast Bioengineering Conference. New Jersey, pp.82–86.

Mattout, J., Henson, R.N. and Friston, K.J. 2007. Canonical source reconstruction for MEG. *Computational Intelligence and Neuroscience*, 2007, pp.67613–10.

Mattout, J., Phillips, C., Penny, W.D., Rugg, M.D. and Friston, K.J. 2006. MEG source localization under multiple constraints: an extended Bayesian framework. *NeuroImage*, 30(3), pp.753–767.

Meijs, J.W., Weier, O.W., Peters, M.J. and van Oosterom, A. 1989. On the numerical accuracy of the boundary element method. *IEEE transactions on bio-medical engineering*, 36(10), pp.1038–1049.

Moran, R.J., Stephan, K.E., Campo, P., Symmonds, M., Dolan, R.J. and Friston, K.J. 2013. Free energy, precision and learning: the role of cholinergic neuromodulation. *Journal of Neuroscience*, 33(19), pp.8227–8236.

Mosher, J.C., Leahy, R.M. and Lewis, P.S. 1999. EEG and MEG: forward solutions for inverse methods. *IEEE transactions on bio-medical engineering*, 46(3), pp.245–259.

Mosher, J.C., Leahy, R.M., Shattuck, D.W. and Baillet, S. 1999. MEG Source Imaging Using Multipolar Expansions. *Lecture Notes in Computer Science*, pp.98–111.

Nolte, G. and Curio, G. 2000. Current multipole expansion to estimate lateral extent of neuronal activity: a theoretical analysis. *IEEE transactions on bio-medical engineering*, 47(10), pp.1347–1355.

Nunez, P.L. 1981. *Electric fields of the brain: The neurophysics of EEG*. New-York: Oxford University Press, pp.83–91.

Penny, W.D. 2012. Comparing Dynamic Causal Models using AIC, BIC and Free Energy. *NeuroImage*, 59(1), pp.319–330.

Pernier, J. 2007. ***Electro et magnéto encéphalographie Biophysique, techniques et méthodes***. Hermès Lavoisier ed. pp.1–248.

Plonsey, R. and Heppner, D.B. 1967. Considerations of quasi-stationarity in electrophysiological systems. *The Bulletin of mathematical biophysics*, 29(4), pp.657–664.

Robillard, P.N. and Poussart, Y. 1977. Specific-impedance measurements of brain tissues. *Medical & Biological Engineering & Computing*, 15(4), pp.438–445.

Rush, S. and Driscoll, D.A. 1968. Current distribution in the brain from surface electrodes. *Anesthesia and analgesia*, 47(6), pp.717–723.

Rush, S. and Driscoll, D.A. 1969. EEG electrode sensitivity--an application of reciprocity. *IEEE transactions on bio-medical engineering*, 16(1), pp.15–22.

Sarvas, J. 1987. Basic mathematical and electromagnetic concepts of the biomagnetic inverse problem. *Physics in Medicine and Biology*, 32(1), pp.11–22.

Schwan, H.P. and Kay, C.F. 1957. Capacitive properties of body tissues. *Circulation research*, 5(4), pp.439–443.

Tuch, D.S., Wedeen, V.J., Dale, A.M., George, J.S. and Belliveau, J.W. 1999. Conductivity mapping of biological tissue using diffusion MRI. *Annals of the New York Academy of Sciences*, 888, pp.314–316.

Tuch, D.S., Wedeen, V.J., Dale, A.M., George, J.S. and Belliveau, J.W. 2001. Conductivity tensor mapping of the human brain using diffusion tensor MRI. *Proceedings of the National Academy of Sciences of the United States of America*, 98(20), pp.11697–11701.

Vallaghé, S. and Clerc, M. 2009. A global sensitivity analysis of three- and four-layer EEG conductivity models. *IEEE transactions on bio-medical engineering*, 56(4), pp.988–995.

Van Uitert, R. and Johnson, C. 2003. Influence of Brain Conductivity on Magnetoencephalographic Simulations in Realistic Head Models. *Proceedings of the 25th Annual International Conference of the IEEE Engineering In Medicine And Biology Society*, pp.1–4.

Vatta, F., Meneghini, F., Esposito, F., Mininel, S. and Di Salle, F. 2010. Realistic and Spherical Head Modeling for EEG Forward Problem Solution: A Comparative Cortex-Based Analysis. *Computational Intelligence and Neuroscience*, 2010(1), pp.1–11.

Wang, Y. and Gotman, J. 2001. The influence of electrode location errors on EEG dipole source localization with a realistic head model. *Clinical neurophysiology : official journal of the International Federation of Clinical Neurophysiology*, 112(9), pp.1777–1780.

Whalen, C., Maclin, E.L., Fabiani, M. and Gratton, G. 2008. Validation of a method for coregistering scalp recording locations with 3D structural MR images. *Human Brain Mapping*, 29(11), pp.1288–1301.

Yvert, B., Bertrand, O., Thévenet, M., Echallier, J.F. and Pernier, J. 1997. A systematic evaluation of the spherical model accuracy in EEG dipole localization. *Electroencephalography and clinical neurophysiology*, 102(5), pp.452–459.